HUMAN GENE THERAPY 23:356–366 (April 2012)

DOI: 10.1089/hum.2011.213

Long-Term Rescue of Retinal Structure and Function by Rhodopsin RNA Replacement with a Single Adeno-Associated Viral Vector in P23H *RHO* Transgenic Mice

Haoyu Mao,[1] Marina S. Gorbatyuk,[2] Brian Rossmiller,[1] William W. Hauswirth,[1,3] and Alfred S. Lewin[1]

Abstract

Many mutations in the human rhodopsin gene (*RHO*) cause autosomal dominant retinitis pigmentosa (ADRP). Our previous studies with a P23H (proline-23 substituted by histidine) *RHO* transgenic mouse model of ADRP demonstrated significant improvement of retinal function and preservation of retinal structure after transfer of wild-type rhodopsin by AAV. In this study we demonstrate long-term rescue of retinal structure and function by a single virus expressing both *RHO* replacement cDNA and small interfering RNA (siRNA) to digest mouse *Rho* and human P23H *RHO* mRNA. This combination should prevent overexpression of rhodopsin, which can be deleterious to photoreceptors. On the basis of the electroretinogram (ERG) response, degeneration of retinal function was arrested at 2 months postinjection, and the response was maintained at this level until termination at 9 months. Preservation of the ERG response in P23H *RHO* mice reflected survival of photoreceptors: both the outer nuclear layer (ONL) and outer segments of photoreceptor cells maintained the same thickness as in nontransgenic mice, whereas the control injected P23H eyes exhibited severe thinning of the ONL and outer segments. These findings suggest that delivery of both a modified cDNA and an siRNA by a single adeno-associated viral vector provided long-term rescue of ADRP in this model. Because the siRNA targets human as well as mouse rhodopsin mRNAs, the combination vector may be useful for the treatment of human disease.

Introduction

Retinitis pigmentosa (RP) is characterized by the progressive loss of peripheral vision, due to the death of rod photoreceptor cells, and potential complete blindness at late stages of the disease, due to the loss of cone photoreceptors. Approximately 40% of RP cases are dominantly inherited and are classified as autosomal dominant retinitis pigmentosa (ADRP). Worldwide, there are almost 1.5 million patients with ADRP who have mutations in 18 different genes (Phelan and Bok, 2000; Hartong *et al.*, 2006). Among these genes, mutations in the rhodopsin (*RHO*) gene account for about 25% of ADRP cases (Daiger *et al.*, 2007; Morris *et al.*, 2009). There are more than 100 *RHO* mutations leading to ADRP, and, although the common cause of retinal degeneration is apoptosis of photoreceptors, different *RHO* mutations lead to apoptosis by different pathways (Mendes *et al.*, 2005). For example, class I mutations fold normally, but are not transported to the outer segment of photoreceptors, and class II mutations do not reconstitute with the 11-*cis*-retinal chromophore readily.

Probably because of a founder effect, the most prevalent *RHO* mutation in North America is P23H (proline-23 substituted by histidine) (Dryja *et al.*, 1990; Daiger *et al.*, 2007). This was the first RP mutation to be identified, and it has been studied extensively both *in vitro* and in animal models (Gorbatyuk *et al.*, 2008; Mao *et al.*, 2011). Investigations in tissue culture indicate that P23H opsin is misfolded and accumulates in the endoplasmic reticulum (Kaushal and Khorana, 1994; Saliba *et al.*, 2002; Noorwez *et al.*, 2003, 2004). In transgenic rats bearing a mouse P23H transgene, levels of the proapoptotic C/EBP-homologous protein (CHOP) are elevated even in a line producing moderate amounts of mutant opsin (Lin *et al.*, 2007), and we have shown that suppressing the unfolded protein response in these animals significantly retards retinal degeneration (Gorbatyuk *et al.*,

[1]Department of Molecular Genetics and Microbiology, University of Florida, Gainesville, FL 32610.
[2]Department of Cell Biology and Anatomy, University of North Texas Health Science Center, Fort Worth, TX 76107.
[3]Department of Ophthalmology, University of Florida, Gainesville, FL 32610.

2010). A P23H knock-in line of mice has been described that recapitulates some of the cardinal histological features of the human disease from the mutation expressed at the normal mouse locus (Sakami *et al.*, 2011). In heterozygous knock-ins, opsin is not detected in the inner segments of photoreceptors suggesting that mutant opsin does not accumulate in the endoplasmic reticulum in the presence of the normal protein. A similar result was reported by Wu and colleagues for P23H transgenic mice (Wu *et al.*, 1998).

Because of the genetic heterogeneity of ADRP, our group and others have explored an approach to gene therapy employing RNA interference (RNAi) or catalytic RNA enzymes (ribozymes) targeting locations in the rhodopsin-coding region that are not specifically associated with ADRP mutations (Kiang *et al.*, 2005; Gorbatyuk *et al.*, 2007a,b; O'Reilly *et al.*, 2007). This allele-independent strategy blocks expression of both the mutant and wild-type genes (Sullivan *et al.*, 2002; Cashman *et al.*, 2005; Kiang *et al.*, 2005; Gorbatyuk *et al.*, 2007a,b, 2008; Chadderton *et al.*, 2009; Smith *et al.*, 2009; Millington-Ward *et al.*, 2011). A similar strategy is being developed by Mussolino and colleagues, who are testing zinc-finger repressors to block the expression of rhodopsin (Mussolino *et al.*, 2011). For therapy, RNA blockade must be combined with replacement genes containing "silent" sequence changes making the resultant mRNA resistant to cleavage. This approach has been taken for treatment of liver disease associated with the *PiZ* allele of α_1-antitrypsin (Li *et al.*, 2011; Mueller *et al.*, 2012). O'Reilly and colleagues (2007) used a single adeno-associated viral (AAV) vector to deliver a small interfering RNA (siRNA) and a resistant *RHO* gene to P23H transgenic mice. Because of the rapid rate of degeneration in this model (Olsson *et al.*, 1992), they were unable to demonstrate functional rescue but did report preservation of some photoreceptors at 10 days, a point at which basic fibroblast growth factor (bFGF) and ciliary neurotrophic factor (CNTF) are still elevated after subretinal injection (Cao *et al.*, 1997). Millington-Ward and colleagues (2011) reported delay of retinal degeneration in P347S *RHO* transgenic mice, using the RNA replacement approach, with a small hairpin RNA (shRNA) and a resistant *RHO* gene, although they used separate viral vectors for the shRNA and for the replacement *RHO* gene, and electroretinogram (ERG) rescue was modest.

Previously, we observed a 50% knockdown of *RHO in vitro* with an siRNA designated 301 and partial rescue of retinal degeneration in P23H transgenic rats using AAV expressing a *RHO*-specific ribozyme (Gorbatyuk *et al.*, 2007a). More recently, we also showed inhibition of retinal degeneration in P23H transgenic mice after AAV delivery of wild-type mouse rhodopsin cDNA that was made resistant to siRNA301 (Mao *et al.*, 2011). This finding suggests that despite the fact that the mutation is genetically dominant, increased production of the wild-type protein can extend the survival of photoreceptors, at least 6 months in mice. Nevertheless, even modest overexpression of wild-type rhodopsin can lead to retinal degeneration in mice (Tan *et al.*, 2001; Mao *et al.*, 2011), and we have therefore pursued the "ablate and switch" approach using the combination of an siRNA and a resistant *RHO* cDNA.

Various *RHO* mutations may cause photoreceptor death either by toxic gain-of-function or a dominant negative mechanism. Stimulation of unregulated phototransduction by mutant rhodopsin or mislocalization of rhodopsin to the nerve terminals might be toxic to rod photoreceptors (Sung *et al.*, 1994; Tan *et al.*, 2001; Tam and Moritz, 2006). In contrast, increased expression of wild-type *RHO* in P23H transgenic mice reduced the rate of retinal degeneration, providing evidence for a dominant negative effect (Frederick *et al.*, 2001). In P23H transgenic or knock-in mice, accumulation of P23H rhodopsin in the rod outer segments suggests that the balance of normal rhodopsin to mutant rhodopsin determines the survival of rod photoreceptor cells (Wilson and Wensel, 2003). On the basis of these studies, we hypothesized that combination of reducing the mutant P23H with siRNA and introducing normal rhodopsin with a resistant cDNA would lead to a more appropriate level of normal rhodopsin expression and a reduced level of P23H rhodopsin (Lewin *et al.*, 1998; Gorbatyuk *et al.*, 2007a; Mao *et al.*, 2011). Our results in P23H transgenic mice show preserved retinal structure for as long as 9 months postinjection, with full recovery of retinal function. The success of this strategy could lead to a treatment of ADRP caused by a variety of rhodopsin mutations.

Materials and Methods

Single AAV construct of RHO301*–siRNA301*

AAV-RS301 contains both siRNA301 and *RHO301*. siRNA301 can cleave both human *RHO* mRNA and endogenous mouse *Rho* mRNA (Fig. 1B). *RHO301* is a resistant form of mouse *Rho* containing five mismatches surrounding the target site in the mouse *Rho* cDNA and includes 109 bp of the 5′ untranslated region (UTR) and 159 bp of the 3′ UTR. Expression of *RHO301* was under the control of a proximal mouse opsin promoter (MOPS) (Flannery *et al.*, 1997). The human H1 promoter was used to direct the expression of siRNA301 as a small hairpin RNA targeting a 19-nucleotide segment of mouse and human opsin mRNAs (Gorbatyuk *et al.*, 2007b). These elements were cloned in a plasmid between AAV2 inverted terminal repeats (Fig. 1A) and the vector was packaged in AAV5 capsids (Zolotukhin *et al.*, 2002).

Animal breeding and injection

P23H transgenic mice on a mouse $Rho^{+/-}$ background and $Rho^{+/-}$ mice were used in this study (Lem *et al.*, 1999; Mao *et al.*, 2011). All the animal procedures were approved by the University of Florida (Gainesville, FL) Institutional Animal Care and Use Committee and were conducted in accordance with the Association for Research in Vision and Ophthalmology (ARVO) *Statement for the Use of Animals in Ophthalmic and Vision Research*. By backcrossing with mouse rhodopsin knockout mice, P23H transgenic mice contain one copy of the human P23H *RHO* transgene and one copy of the mouse endogenous *Rho*P23H (*RHOP23H*,$Rho^{+/-}$). We also crossed rhodopsin knockout mice with C57BL6/J mice to obtain control mice with the $Rho^{+/-}$ genotype. All the mice were kept under specific pathogen-free (SPF) conditions with a daily cycle of 12 hr of light and 12 hr of dark.

We injected 1 μl of the AAV2/5-RHO301-siRNA301 (RS301) virus at 1×10^{12} vector genomes/ml into the subretinal area of the eyes on postnatal day 15 (P15) (Timmers *et al.*, 2001). The injection was performed on either P23H

transgenic mice (*RHOP23H,Rho*$^{+/-}$) or control mice (*Rho*$^{+/-}$). Animals were anesthetized with ketamine–xylazine combination solution in sterile saline. One drop of 1% atropine sulfate and 2.5% phenylephrine were applied for dilation of pupils and proparacaine was administered as a local anesthetic. Some mice had right eyes injected with AAV2/5-RS301 and left eyes uninjected. Other mice had right eyes injected with AAV2/5-RS301 and left eyes injected with same volume and titer of control virus expressing humanized green fluorescent protein (GFP) under the control of the MOPS promoter delivered by AAV2/5.

Immunodetection of rhodopsin

At 1 month postinjection, P23H transgenic mice were killed, and retinas were extracted from the eyes. We chose this interval because most of the photoreceptors are still intact at this stage. Protein samples were prepared by ultrasound disruption in Laemmli sample buffer containing 2-mercaptoethanol (Laemmli, 1970). The Pierce Biotechnology bicinchoninic acid (BCA) protein assay was performed to estimate the concentration of total protein from each retina (Thermo Scientific, Rockford, IL). Thirty micrograms of protein was diluted in a 30-μl total volume to load onto sodium dodecyl sulfate (SDS)–polyacrylamide gels (12% acrylamide). After electrophoresis, an iBlot dry blotting system (Life Technologies, Carlsbad, CA) was used to transfer the proteins onto polyvinylidene difluoride (PVDF) membranes. To detect the rhodopsin protein we used a C-terminal mouse rhodopsin monoclonal antibody, 1D4, which detects both mouse rhodopsin and human rhodopsin (a generous gift from R. Molday, University of British Columbia, BC, Canada), and a rabbit antibody to β-actin as a recovery and loading control. Anti-mouse secondary antibody was used to detect 1D4–rhodopsin complexes, and anti-rabbit secondary antibody was used to detect the β-actin antibody. After secondary antibody staining, we analyzed the blot with an ODYSSEY scanner (LI-COR, Lincoln, NE). Rhodopsin content was normalized to the level of endogenous β-actin expression.

RNA extraction and detection

Mice were killed at 1 month postinjection to extract RNA from retinas, using TRIzol reagent (Life Technologies). We used RNase-free DNase I (Ambion, Austin, TX) to purify RNA samples. The final concentration of each sample was determined by absorbance at 260 nm.

A first-strand cDNA synthesis kit (GE Healthcare, Piscataway, NJ) was used to produce cDNA from mouse *Rho*, P23H human *RHO*, and AAV-delivered *RHO301*. Primer 5′-CCATGGCAGTTCTCCATGCT-3′ was used for both human and mouse *Rho* exon 1 and primer 5′-TTCTCCCCG AAGCGGAAGTT-3′ (*RHO* exon 2) was used as the reverse primer. A GenElute PCR clean-up kit (Sigma-Aldrich, St. Louis, MO) was used to purify PCR products. Preliminary experiments determined that 22 cycles was in the linear range of amplification for both cDNAs. Because *RHO301* is specifically susceptible to digestion with the endonuclease *Mse*I, this enzyme was used to distinguish the *RHO301* PCR product from the endogenous mouse and human PCR products. Digestion of the *RHO301* PCR product resulted in two bands of 283 and 70 bp, but products of the endogenous mouse and human products resulted in one band of 353 bp. PCR products were detected by SYBR green staining and scanning with a Storm PhosphorImager (GE Healthcare), and their intensity was analyzed with Quantity One software (Bio-Rad, Hercules, CA) using area-under-the-curve measurements. β-Actin PCR products were used as endogenous control to normalize the intensity of *RHO* products.

Fundus imaging

The Micron III fundus microscope (Phoenix Research Laboratories, Pleasanton, CA) was used to obtain digital images of the central retina. Mice were anesthetized with ketamine and xylazine. The eyes were dilated with 1% atropine sulfate and 2.5% phenylephrine. After the pupils were dilated, one drop of 2.5% methylcellulose eye drops was applied to limit refraction. Fundus images were captured at 1 and 9 months postinjection.

Electroretinography

P23H transgenic mice and control mice were analyzed by simultaneous, full-field electroretinography (ERG) as described previously (Mao *et al.*, 2011). Briefly, dark-adapted mice were anesthetized, and their eyes were dilated under dim red light conditions. Scotopic ERG responses from both dilated eyes were recorded with an LKC electrodiagnostic system (LKC Technologies, Gaithersburg, MD). Both a-wave and b-wave amplitudes were measured 1, 2, 3, 6, and 9 months postinjection to analyze the retinal function of RS301-injected eyes in comparison with either uninjected contralateral eyes or AAV5-MOPS-GFP-injected eyes. Scotopic ERGs, which measure primarily rod function, were elicited with 10-msec flashes of white light at –20, –10, and 0 dB with a 5-sec delay between flashes for low light intensities and a 1-min delay at 0 dB (0 dB = 2.5 cd·sec/m^2, –10 dB = 0.25 cd·sec/m^2, and –20 dB = 0.025 cd·sec/m^2). Five scans were averaged at each light intensity. Figure 4, showing the results at 0 dB, the highest light intensity, represents a mixed rod and cone response. Supplementary Fig. S2 (supplementary data are available online at www.liebertonline.com/) reports the results at –20, –10 and 0 dB, and shows a rod-specific response from –20 dB. The a-wave amplitudes were measured from baseline to peak in the cornea-negative direction, and b-wave amplitudes were measured from the cornea-negative peak to the major cornea-positive peak. The results from each group of mice were averaged and the means were compared statistically, using a Student *t* test for paired data, when comparing treated and control eyes from the same mice. For comparison of the mean amplitudes of multiple groups, we employed one-way analysis of variance (ANOVA).

Spectral domain optical coherence tomography image and measurement

We performed spectral domain optical coherence tomography (SD-OCT) imaging at 3, 6, and 9 months postinjection to analyze changes in retinal structure in living mice. A Bioptigen SD-OCT instrument (Bioptigen, Research Triangle Park, NC) was employed for image capture and measurement of the outer nuclear layer (ONL) thickness. (This instrument was not yet available to us at the 1-month time

point.) During the OCT recording, mice were anesthetized, and the pupil was dilated as described for funduscopy. One hundred linear B-scans were obtained, and 20 images were averaged to minimize the background and to achieve higher resolution. ONL thickness was measured by rectangular scan pattern to capture the image from the sequences of horizontal scan lines. We recorded four measurements at the same distance from the optical nerve head from each eye and used these data to determine the average final ONL thickness.

Morphology analysis

For histology analysis, mice were killed 9 months postinjection, and freshly isolated retinas were immersed in 2% paraformaldehyde plus 2.5% glutaraldehyde. Retinas were postfixed in 1% osmium tetroxide at 4°C for 4 hr and then maintained in 0.1 *M* cacodylate buffer overnight. Retinas were dehydrated through a graded series of ethanol baths and then were embedded in an epoxy resin. Tissue sections (1 μm) were made along the vertical meridian through the optic disc and stained with toluidine blue. Estimation of the length of the outer segments was done by measuring the contour lengths of 10 individual outer segments at each of 10 evenly spaced locations (5 superior loci and 5 inferior loci) along the vertical meridian, using a $\times 40$ objective with a Stereo Investigator (MBF Bioscience, Williston, VT) connected to a Zeiss microscope. The measurements were averaged from 10 readings at each location.

Flow cytometry analysis

To study the *RHO301* resistance to siRNA301, we transfected HEK293 cells with *RHO301–GFP* and *RHO–GFP* (C-terminal fusion genes). Cells were cotransfected with siRNA301 or a control irrelevant siRNA. After 48 hr, relative fluorescence intensities of GFP expression were examined by flow cytometry.

Statistical analysis

Statistical analyses were performed by Student *t* test for paired groups, and by ANOVA for multiple comparisons. A *p* value less than 0.05 was considered statistically significant. All data are shown as means ± SEM for comparison.

Results

Delivery of both siRNA301 and RHO301 *in a single AAV virus*

We prepared a single AAV construct containing both siRNA301, which cleaves mouse and human *RHO* mRNA at nucleotide 301 (human numerology), and *RHO301*, a "hardened" cDNA with five silent base changes surrounding position 301 (Fig. 1A and B). The resistance of *RHO301* to siRNA301 was documented in cell transfection assays (Supplementary Fig. S1). We had previously tested these components separately in rat and mouse models of ADRP (Gorbatyuk *et al.*, 2008; Mao *et al.*, 2011). When delivered as an shRNA, siRNA301 leads to a 60% reduction in mouse *Rho* mRNA and a proportional reduction in ERG a-wave amplitudes. AAV delivery of resistant *RHO301* cDNA leads to a 50% increase in total rhodopsin protein and arrests retinal degeneration in P23H *RHO* transgenic mice on the mouse $Rho^{+/+}$ background. Here we delivered the combined cDNA and shRNA, in a single AAV2 vector pseudotyped with AAV5 capsid proteins, to P23H transgenic mice on a $Rho^{+/-}$ background (Fig. 1A). AAV5 leads to widespread transduction of photoreceptors in the mouse (Fig. 1C), and using the mouse opsin promoter, transduction is specific for photoreceptors (Gorbatyuk *et al.*, 2005). Our ADRP model consisted of P23H transgenic mice, which contain one insertion of the P23H human *RHO* transgene and one copy of the wild-type mouse *Rho* gene. (The human gene is designated *RHO*, whereas the mouse gene is designated *Rho*.) One microliter of the single AAV2/5-RHO301-siRNA301 (RS301) virus was injected on postnatal day 15 (P15) into right eyes, and the left eyes were either untreated or were injected with control virus AAV2/5-MOPS-GFP, which had no influence on retinal function in the mice (Mao *et al.*, 2011). Expression of siRNA301 as a small hairpin RNA was driven by an H1 promoter, and *RHO301* was under the control of approximately 500 bp of the mouse opsin proximal promoter (MOPS500).

We called the combination virus expressing the siRNA and resistant mRNA AAV-RS301. To verify the successful delivery of siRNA301–*RHO301*, mRNA and protein levels of rhodopsin expression were determined by reverse transcription-PCR and immunoblotting with the C-terminal rhodopsin-specific antibody 1D4 (Figs. 2 and 3). We delivered siRNA301 to suppress both the P23H human and endogenous mouse wild-type rhodopsins, and we analyzed the mRNAs of both *RHO* transcripts. Both of these RNA species were decreased, in right, AAV5-RS301-injected eyes, and mRNA of the "hardened" form of mouse *Rho* (*RHO301*) was present only in right eyes injected with AAV-RS301 and not in left, uninjected eyes. The same primer set was used to amplify the endogenous mRNA (mouse and P23H) and the AAV-delivered *RHO301* mRNA, but the silent mutations introduced an *Mse*I endonuclease site that permitted the *RHO301* to be distinguished, resulting in bands of 283 and 70 bp (Fig. 2A). In the same lane, depletion of the largest band (353 bp) indicated reduction of the endogenous mRNA caused by delivery of siRNA301. All the bands were normalized to corresponding β-actin amplification bands (Fig. 2B and C). Even though there was a significant depletion of endogenous rhodopsin mRNA (74%) (Fig. 2B), with the contribution of *RHO301*, the total *RHO* mRNA level from right AAV5-RS301-injected eyes was significantly higher than that of contralateral uninjected eyes from same group of P23H transgenic mice. More than a 2-fold increase in total *RHO* mRNA was obtained by single AAV delivery of RHO301-siRNA301 (Fig. 2C) ($p < 0.05$).

Western blots of rhodopsin proteins were performed at the same time point and also indicated a 2-fold increase in rhodopsin content in eyes treated with AAV-RS301 ($p < 0.05$). Rhodopsin antibody 1D4 was applied to protein extracts from left uninjected retinas and right AAV-RS301-injected retinas (Fig. 3A). Endogenous β-actin was used for normalization of opsin levels. For the rhodopsin dimer, we observed a 50% increase in AAV-RS301-injected eyes relative to uninjected eyes, but this increase was not statistically significant (Fig. 3B).

Long-term rescue of retinal function by a single injection of AAV-RS301

To detect retinal function in P23H transgenic mice or nontransgenic control mice, scotopic ERG was performed at

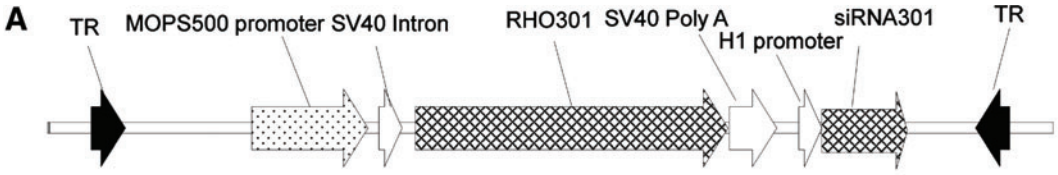

B

Target sequences of rhodopsin to siRNA301		
Name	Target sequences	Cleavage by siRNA301
Human RHO	CTTCCTCACGCTCTACGTC	Yes
Mouse RHO	CTTCCTCACGCTCTACGTC	Yes
RHO301	CTTC**T**T**A**AC**CT**T**G**TACGTC	No

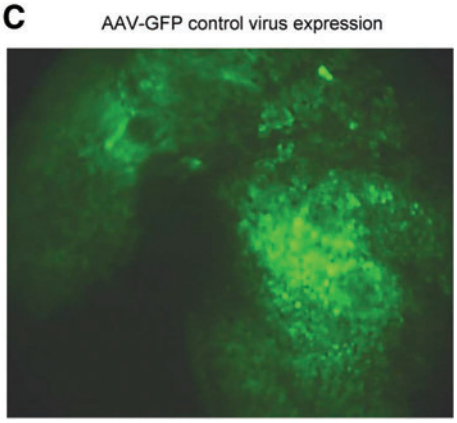

FIG. 1. A single AAV vector expresses both *RHO301* and siRNA301. **(A)** Map of AAV5-RHO301-siRNA301 (AAV-RS301). The expression of *RHO301* was controlled by the proximal promoter region of the mouse opsin gene (MOPS500), and the small hairpin RNA containing the siRNA was controlled by the human H1 promoter. The entire coding region was contained between AAV2 terminal repeats (TR) and packaged in AAV5 capsids. **(B)** Various target sequences of human rhodopsin, mouse rhodopsin, and a resistant version of mouse rhodopsin (*RHO301*). **(C)** Subretinal injection of AAV2/5-MOPS-GFP leads to widespread transduction of the retina. One month after injection of our control virus, AAV-MOPS-GFP expression of GFP could be detected in a large area of the retina in a living mouse, using a Micron III fundus microscope equipped with a fluorescein filter. Color images available online at www.liebertonline.com/hum

1, 2, 3, 6, and 9 months postinjection at intensities of 0, –10 and –20 dB. The high-intensity responses (0 dB) reported in Fig. 4 reflect the mixed rod and cone response. Mice were injected with AAV5-RS301 via their right eyes and with AAV-MOPS500-GFP via their left eyes (Fig. 4). No difference in ERG response was found in comparing *GFP*-injected eyes with uninjected eyes over a 9-month time course (data not shown). The ERG a-wave is a negative deflection that directly measures the response of photoreceptor cells to flashes of light. By 1 month postinjection (45 days after birth), the

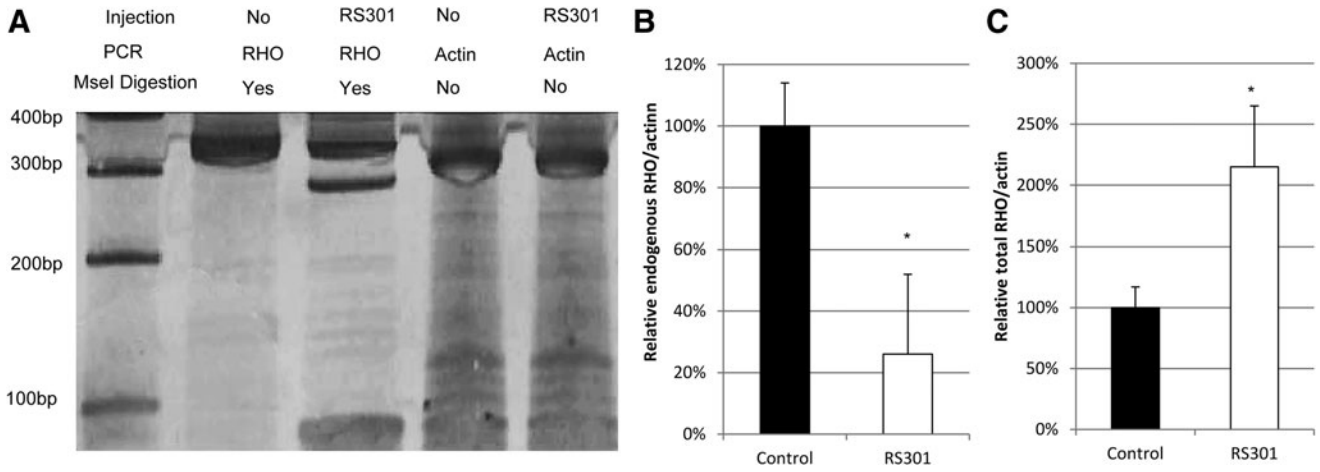

FIG. 2. Subretinal injection of AAV-RS301 leads to an increase in total rhodopsin RNA. **(A)** Reverse transcription (RT)-PCR products of mouse and human rhodopsin mRNAs were prepared with a common set of primers in the same reaction (Mao *et al.*, 2011). Subsequent incubation with restriction enzyme *Mse*I digested *RHO301* into bands of 283 and 70 bp, and undigested human P23H *RHO* and mouse *Rho* had the same 353-bp band. RT-PCR products from uninjected eyes contained only the uncut 353-bp product after *Mse*I treatment. Amplification products of β-actin mRNA from the same retinas (without *Mse*I digestion) were used for normalization. **(B)** Endogenous rhodopsin mRNA levels (human P23H *RHO* and mouse *Rho*) were reduced in RS301-treated eyes (open column) ($p < 0.05$; $n = 3$). **(C)** Total rhodopsin mRNA (human P23H *RHO*, mouse *Rho*, and *RHO301*) increased in RS301-injected eyes (open column) ($p < 0.05$; $n = 3$). In **(B)** and **(C)** the ratio of rhodopsin to actin PCR products in untreated eyes was set to 100%.

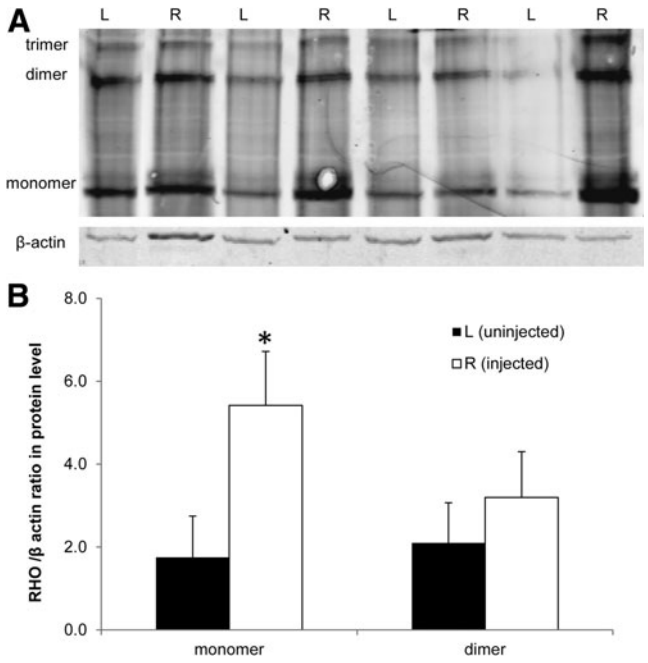

FIG. 3. Increased rhodopsin protein in P23H transgenic eyes injected with AAV-RS301. Four P23H transgenic mice injected with AAV-RS301 in right (R) eyes and uninjected in their left (L) eyes were analyzed by immunoblot. **(A)** Image of anti-rhodopsin staining using C-terminal specific antibody 1D4. Protein levels were normalized to β-actin protein from the same eye. **(B)** Quantification of image **(A)**, demonstrating increased RHO protein content in injected right eyes (open columns) compared with uninjected left eyes (solid columns) ($n = 4$; $^*p < 0.05$).

a-wave amplitude in AAV-RS301-injected eyes (308 μV) was twice that of AVV-GFP-infected eyes (155 μV). Although the amplitudes declined between 1 and 2 months postinjection, RS301-treated photoreceptors remained twice as responsive as those in control injected eyes (195 to 95 μV). By 3 months, the response in the RNA replacement eyes remained constant, whereas the ERG a-wave in the AAV-GFP-treated eyes continued to decline, so that the difference between eyes was nearly 4-fold. By 6 and 9 months, the a-wave response was more than 6-fold greater in treated eyes than in control eyes ($p < 0.005$ at 1, 3, 6, and 9 months postinjection, and $p < 0.05$ at the 2-month time point). The latency (implicit time) of the a-wave response increased with age in the P23H transgenic mice after control treatment (Supplementary Fig. S2) (Mao *et al.*, 2011). However, after treatment with AAV-RS301, the implicit time of the a-wave remained relatively constant, and the difference from control treated eyes was significant at each interval ($p < 0.005$). Sample waveforms from control treated and RS301-treated eyes are shown in Supplementary Fig. S2B.

The positively inflected b-wave measures the response of second-order neurons to a light flash. The b-wave amplitudes in RS301-treated eyes (760 μV) were twice those in the *GFP*-treated eyes at 1 month postinjection (Fig. 4B). By 2 months, the b-wave amplitudes in RS301-treated eyes had declined to 550 μV, where they remained for the duration of the 9-month study. However, the amplitude in AAV-GFP-injected eyes had declined to 200 μV by 2 months and continued to decline, so that by 9 months there was a 5-fold difference in b-wave amplitude between treated and control eyes ($p < 0.005$ at 1, 2, 6, and 9 months postinjection, and $p < 0.05$ at the 3-month postinjection time point).

The rod-specific response, recorded at –20 dB intensity, indicated preservation of rod-specific function at 9 months postinjection with the a-wave amplitude more than twice that of control treated eyes (Supplementary Fig. S3). At this stimulation intensity, RS301-injected eyes maintained amplitudes of 300 μV from 1 month until 9 months postinjection, and this level was significantly higher than that of control injected eyes at the same ages ($p < 0.05$ at 1 month, $p < 0.005$ at 9 months) (Supplementary Fig. S3B and D).

In a parallel comparison, the ERG response was compared among RS301-treated eyes and uninjected contralateral eyes of both P23H transgenic and heterozygous *Rho* knockout ($Rho^{+/-}$) mice (Fig. 4C and D). This is the genetic background of the P23H transgenic mice in this study. At 1 month, we observed a 40% reduction ($p < 0.05$) in the a-wave response in the injected eyes of nontransgenic mice ($Rho^{+/-}$). We attribute this reduction to residual effects of retinal detachment caused by injection. However, this decrease was temporary, and by 9 months the difference in amplitude between uninjected and injected eyes of nontransgenic mice was only 20% and was not statistically significant. There was no significant difference in the b-wave amplitudes between the injected and uninjected eyes of nontransgenic mice at either time point. For the P23H transgenic mice, the a-wave and b-wave amplitudes of the uninjected eyes were significantly lower than the amplitudes of RS301-treated eyes at 1 month (40% for a-wave and 50% for b-wave; $p < 0.05$) and especially at 9 months, when the a- and b-wave amplitudes were five times lower than for eyes treated with AAV-RS301 ($p < 0.05$). The ERG amplitudes of the treated P23H eyes were not different from those of uninjected $Rho^{+/-}$ mice at either time point.

Retinal structure is preserved in RHO301–*siRNA301-treated P23H mice*

Integrity of the retina was measured by spectral domain optical coherence tomography (SD-OCT), a noninvasive method that allows imaging of the retinal microstructure (Huber *et al.*, 2009). Representative images from 3, 6, and 9 months postinjection illustrate the thinning of the outer nuclear layer (ONL) in AAV-GFP-treated left eyes compared with AAV-RS301-treated right eyes (Fig. 5A). The ONL, which contains the nuclei and cell bodies of photoreceptor cells, was measured between bright lines representing the inner plexiform layer and the outer limiting membrane in these images. ONLs from control treated retinas were significantly thinner by the 3-month time point and remained, on average, half as thick as the retinas treated with RS301 ($p < 0.005$) (Fig. 5A and B). The SD-OCT image at 9 months of retinal degeneration also revealed inhomogeneity in the inner/outer segment layer, and potential subretinal detachment in the left eyes. The ONL thickness of the RS301-treated eyes was similar to that of wild-type mice at the same ages (Supplementary Fig. S4).

Digital fundus imaging was done to observe pathological changes at the surface of retinas of P23H mice (Fig. 5C). At 1 month postinjection of GFP control virus, no significant

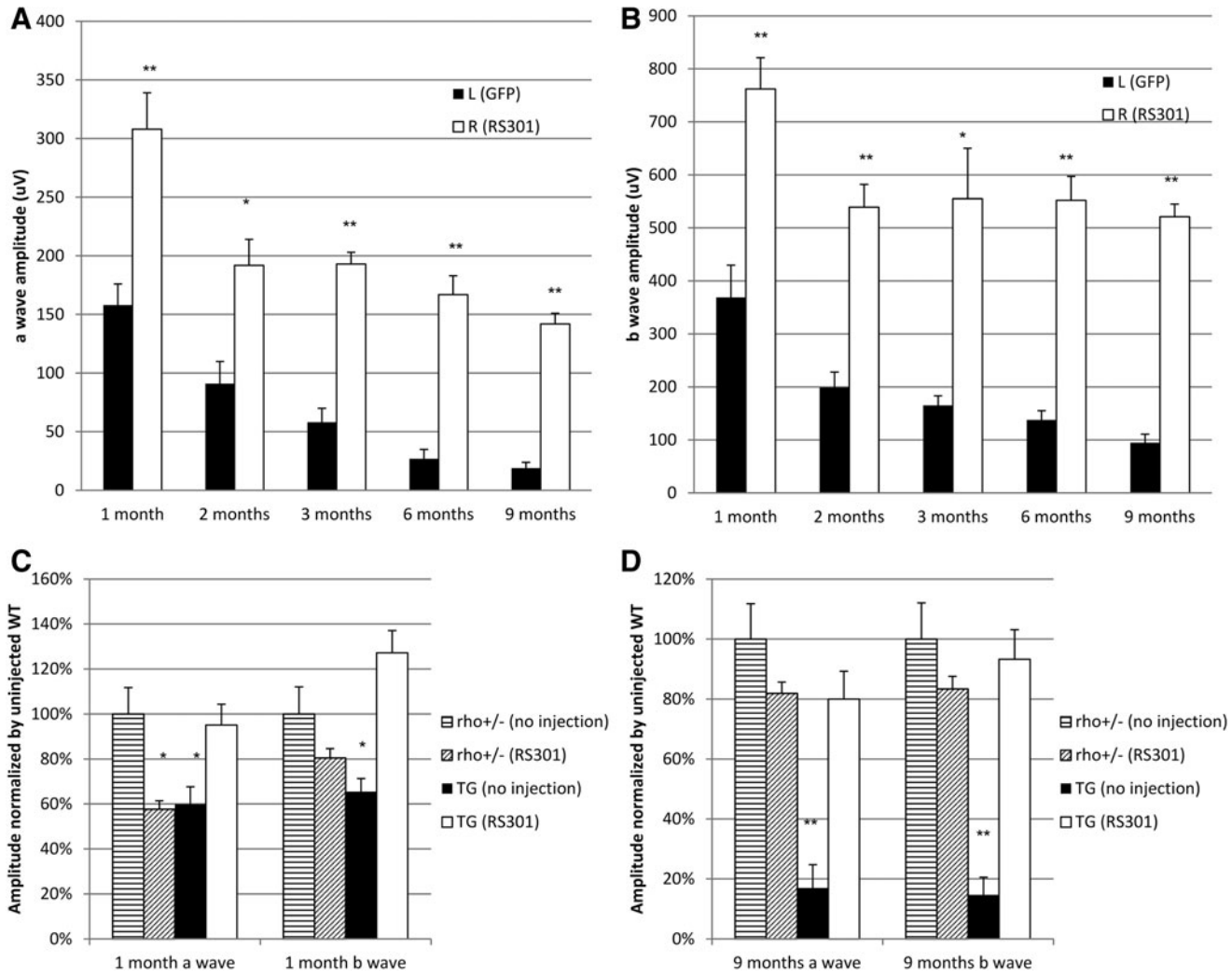

FIG. 4. *RHO301*–siRNA301 gene transfer rescued retinal function in P23H transgenic mice. **(A)** a-wave amplitudes were measured 1, 2, 3, 6, and 9 months postinjection. The data presented here are from high-intensity flashes (0 dB) and represent both rod and cone responses. AAV-RS301-injected eyes exhibited a significantly increased a-wave response at all time points compared with control injected eyes (AAV-GFP) ($n=9$, $^{**}p<0.005$ at 1, 3, 6, and 9 months; $p<0.05$ at 2 months). **(B)** b-wave amplitudes are presented from 1, 2, 3, 6, and 9 months postinjection. Right AAV-RS301-injected eyes showed a significantly increased b-wave response compared with left AAV5-GFP-treated eyes ($n=9$ at 1, 2, 6, 9 months; $^{**}p<0.005$ at 3 months, $^{*}p<0.05$). To determine the extent of rescue of ERG amplitudes in P23H eyes relative to untreated wild-type eyes, we compared a-wave and b-wave amplitudes in P23H transgenic mice with those of nontransgenic mice at 1 month postinjection **(C)** and 9 months postinjection **(D)**. Left eyes of both strains were untreated and right eyes were injected with AAV-RS301. ERG amplitudes of the untreated nontransgenic eyes were set at 100% for both time points. At 1 month, both the uninjected transgenic and injected nontransgenic eyes showed a statistically significant ($^{*}p<0.05$) decrease in a-wave amplitude. However, by 9 months only the untreated P23H transgenic eyes showed a significantly diminished response in both a- and b-wave amplitudes, $<20\%$ that of the untreated, nontransgenic eyes ($n=7$; $^{**}p<0.005$). P23H eyes injected with AAV-RS301 maintained 80% of the a-wave amplitude of untreated nontransgenic eyes ($p>0.05$). For the b wave, P23H eyes injected with AAV-RS301 maintained almost 95% of the amplitude of the uninjected, nontransgenic eyes.

morphological changes were found in the eyes, except for a pigmented patch near the optic disc seen in some retinas. In contrast, P23H eyes with AAV-RS301 treatment had a normal retinal appearance at 1 month, and this normal fundus was maintained for 9 months. However, at 9 months postinjection, the control injected eyes had severe damage visible in the fundus image. Evidence of pathological processes included a hypopigmented patch, loss of pigment in a region next to optic disc but a hyperpigmented region beneath it, and many pale spots distributed across the retina (Fig. 5C). The preservation of retinal structure observed in SD-OCT and fundus images was in accordance with the rescue of the ERG response observed in RS301-treated eyes.

Because it was difficult to measure the dimensions of the rod outer segments by OCT, after the 9-month time point, mice were humanely killed and their retinas were prepared for microscopic examination in plastic sections (Fig. 6A). Images of retinal sections were consistent with the results of SD-OCT for both injections. Significantly shorter outer segments (OSs) were detected in AAV-GFP control retina

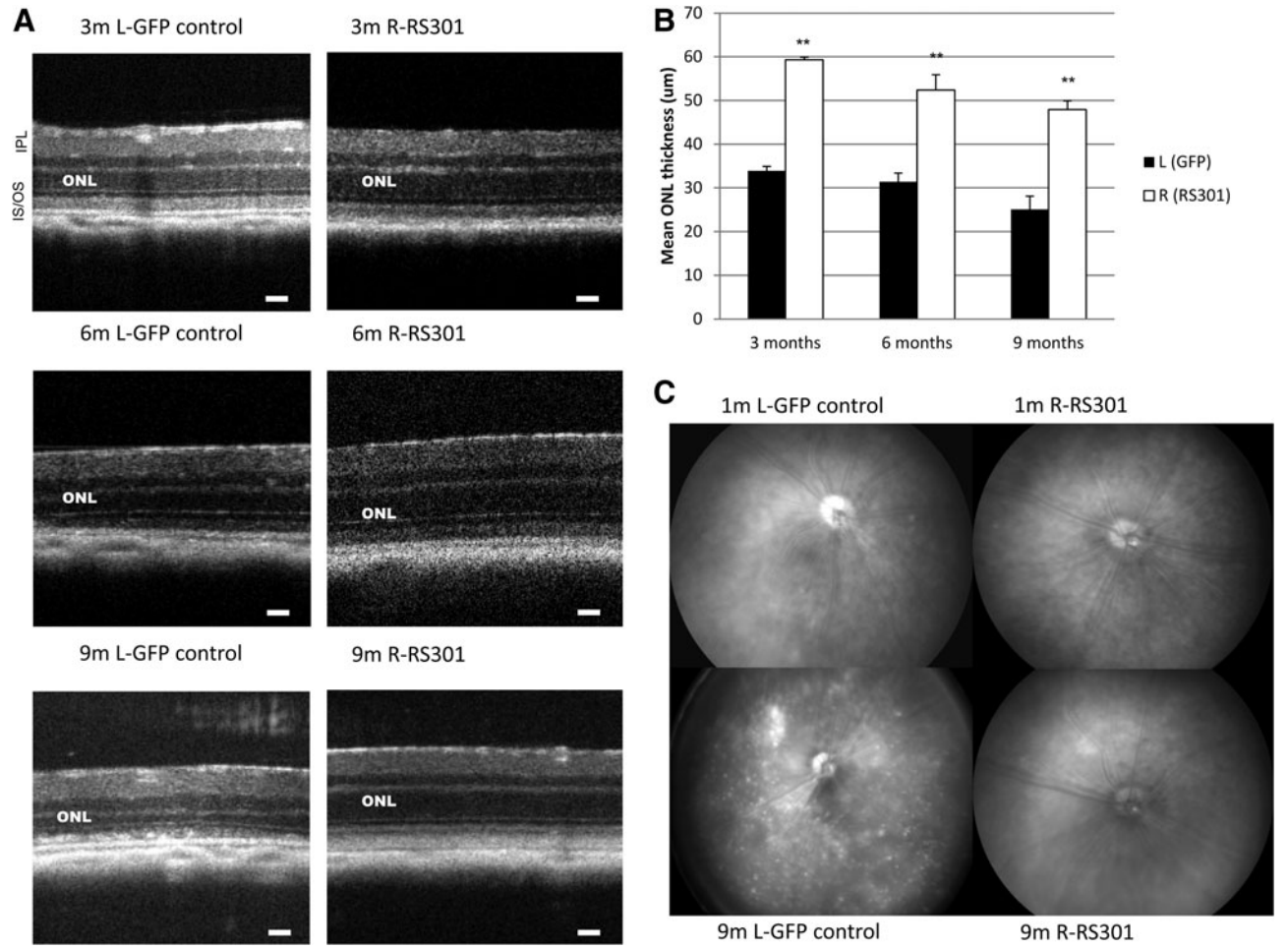

FIG. 5. Injection of AAV-RS301 preserved retinal structure and morphology in P23H transgenic mice. **(A)** Spectral domain optical coherence tomography (SD-OCT) images were captured in live mice at the 3-, 6-, and 9-month postinjection time points. Scale bars: 30 μm. **(B)** The thickness of the outer nuclear layer (ONL) was measured from SD-OCT images at four standard locations relative to the optic nerve head at 3, 6, and 9 months postinjection. The thickness of the ONL from right AAV-RS301-injected eyes was significantly greater than that from left AAV-GFP-injected eyes at corresponding time points ($n=9$; $^{**}p<0.005$ at 3, 6, and 9 months). **(C)** Fundus images were captured at 1 and 9 months postinjection. *Top left:* A P23H transgenic mouse 1 month postinjection of AAV-GFP. Pigmentary changes were observed in the area near the optic nerve head (at 7 o'clock in this image). *Top right:* Normal appearance of the fundus in the AAV-RS301 contralateral eye. *Bottom left:* Significant bleaching and pigmentary irregularities in the retina of a control P23H eye treated with the control virus. Many white spots were present in the retina, with one hyperpigmented region near the optic nerve head. The optic nerve head was also pale in the control treated eyes. *Bottom right:* An image of an AAV-RS301-treated right eye. The fundus picture appears similar to the 1-month postinjection picture. IPL, inner plexiform layer; IS/OS, inner segment/outer segment interface.

compared with AAV-RS301-treated retina (Fig. 6A–C). The differences in length of outer segments were more pronounced in the inferior hemisphere of the retina. Combining the results from the whole retina, outer segments were significantly longer in RS301-treated eyes than in *GFP* control eyes ($p<0.005$) (Fig. 6C). This result confirmed the preservation of retinal structure with RS301 treatment as detected *in vivo* by SD-OCT (Figs. 5 and 6).

Discussion

With a single dose of AAV2/5-RHO301-siRNA301 (AAV-RS301) in a single virus, we observed long-term preservation of normal retinal function and normal retinal dimensions and morphology, including preservation of photoreceptor cells. AAV delivery of the wild-type *RHO* cDNA, *RHO301*, arrested retinal degeneration in P23H transgenic mice on a mouse $Rho^{+/+}$ background (Mao *et al.*, 2011), but in this study we employed P23H transgenic mice with one copy of the P23H transgene and one copy of the mouse rhodopsin gene, and these mice exhibited a faster rate of degeneration; supplementing with the wild-type gene reduced at 1 month, but did not arrest, degeneration of photoreceptors in this model at later time points (Supplementary Fig. S5). Consequently, in the present study we used this combination vector to test the hypothesis that a suppression and replacement strategy is sufficient to fully rescue photoreceptors in the P23H transgenic ADRP model.

Total rhodopsin RNA and protein contents of treated eyes were significantly elevated after injection of RS301 (Figs. 2 and 3). By ERG, from 1 to 9 months postinjection, we observed a dramatic increase in both a- and b-wave amplitudes

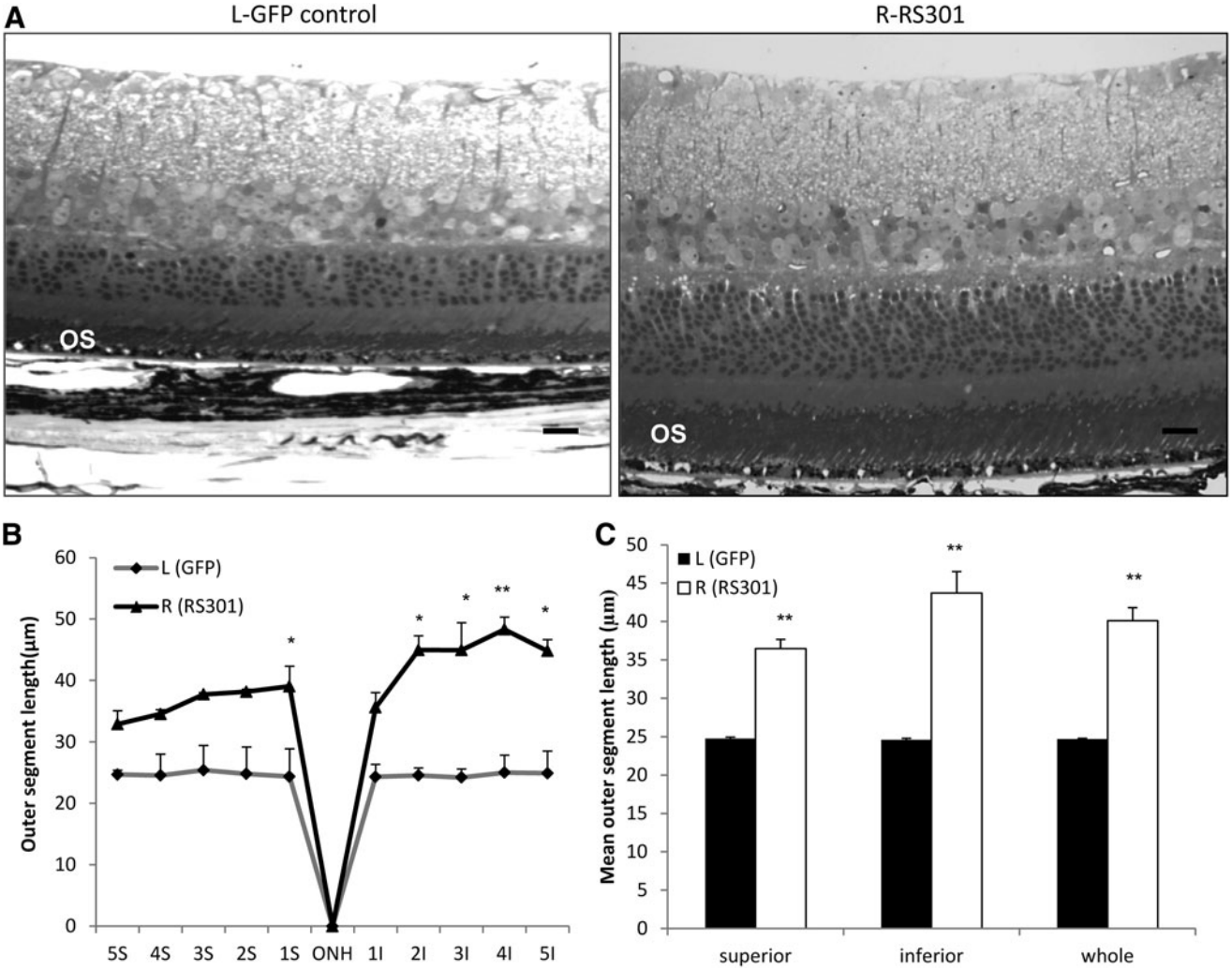

FIG. 6. Histological preservation of retinas after 9 months of treatment with AAV-RS301. **(A)** Semithin sections were imaged 9 months postinjection. *Left:* Image of a retina from a P23H transgenic eye treated with AAV-GFP. In accordance with the *in vivo* image from SD-OCT, the image reveals a thin ONL (five or six rows of nuclei, with numerous gaps). This image also reveals shortened rod outer segments (OS). Scale bar: 30 μm. *Right:* In eyes treated with AAV-RS301, retinal structure was well preserved with a thicker whole retina, ONL, and OS. **(B)** The contour lengths of outer segments analyzed at 10 positions across the retina revealed longer outer segments at each position analyzed (S, superior hemisphere; I, inferior hemisphere). In five superior locations near the optic nerve head and five inferior locations, the differences between control treated and RS301-treated eyes were significantly different ($n = 4$; $^*p < 0.05$, $^{**}p < 0.005$). **(C)** OS length was analyzed in whole superior area, whole inferior area, and whole retina including both superior and inferior areas to determine the overall length of OSs ($n = 4$; $^{**}p < 0.005$). ONH, optic nerve head.

in RS301-treated eyes relative to control treated eyes that reached 6-fold for the a-wave amplitudes and 5-fold for b-wave amplitudes (Fig. 4). This level of ERG response was approximately 80% of a-wave and 95% of b-wave amplitudes of nontransgenic mice (Fig. 4C and D). Moreover, the expression of *RHO301*-siRNA301 in nontransgenic mice did not cause permanent damage to the retina, as demonstrated by the finding that 80% of a- and b-wave amplitudes were maintained at the 9-month postinjection stage (Fig. 4C and D). Even though we estimated a 2-fold increase in total rhodopsin RNA and protein content in treated eyes (Figs. 2 and 3), the ERG levels that we measured were equivalent to those of $Rho^{+/-}$ mice (Fig. 4C and D). This apparent discrepancy may reflect the negative impact of residual P23H rhodopsin in photoreceptors (Wilson and Wensel, 2003) or simply the fact that not all of the RNA and protein we measured by molecular techniques corresponded to functional rhodopsin. Preservation of ERG amplitudes is explained by the improved survival of photoreceptor cells in RS301-treated eyes: at 9 months postinjection, ONL and OS thicknesses were significantly increased in treated versus control treated eyes, based on SD-OCT and morphometric analyses (Figs. 5 and 6), and the appearance of the retinal surface supported the findings of normality of the RS301-treated retinas compared with the thinning of the retina in *GFP*-treated control eyes at the same late stage (Fig. 5C).

We developed this RNA replacement approach to be allele independent, given that more than 100 mutations of *RHO* are

associated with ADRP. In this paper, we have established the success of that approach for only one of these mutations. A similar suppression and replacement strategy for the treatment of ADRP was also reported by another group, using the P347S *RHO* transgenic mouse (Chadderton *et al.*, 2009; Millington-Ward *et al.*, 2011). They demonstrated short-term rescue of retinal structure (three or four rows of nuclei in the ONL, approximately 40% of the wild type) and modest rescue of the ERG response (b-wave amplitudes of 60 μV at 20 weeks, compared with 500 μV at 38 weeks in this study), using separate AAV vectors for delivery of the siRNA and the replacement cDNA. The two-virus approach permits balancing of the shRNA and the replacement gene by varying the ratio of vectors. Although photoreceptors can be coinfected with two viruses, our approach ensures that a photoreceptor receiving the siRNA also receives the replacement gene. Another major difference between their study and ours, however, is the animal model. As noted previously, different rhodopsin mutations kill photoreceptors by different pathways. Because it is not properly targeted to the outer segment, P347S rhodopsin probably kills rods by a toxic gain-of-function mechanism (Wilson and Wensel, 2003; Mendes *et al.*, 2005). We and Frederick and colleagues (Frederick *et al.*, 2001; Mao *et al.*, 2011) have presented results suggesting that P23H rhodopsin can be overcome by increased expression of normal rhodopsin, indicating that the P23H protein is not in itself toxic. It is not unreasonable to assume that the level of RNA replacement needed for suppression of a gain-of-function mutation is higher than that required for a dominant-negative mutation. O'Reilly and colleagues (2007) attempted gene therapy of P23H transgenic mice with AAV expressing both an siRNA and a replacement rhodopsin. They used a rapidly degenerating transgenic mouse line and could demonstrate short-term (10-day) effects only by grouping the highest and lowest 15% of ONL measurements for analysis. We have spent years developing and backcrossing mouse lines with a human P23H transgene that degenerate at a moderate rate (see black columns in Fig. 4), and this has allowed unbiased (panretinal) assessment of the impact of gene therapy by RNA replacement.

AAV is a good choice for stable delivery of siRNA and replacement gene together in a single virus. Li and colleagues have demonstrated the effectiveness of this single-vector RNA replacement approach, using AAV8 in an animal model of liver disease associated with the human *PiZ* allele of α_1-antitrypsin (Li *et al.*, 2011). Because of the efficiency of gene transfer to photoreceptors with AAV2/5, this vector system enabled us to transfer both siRNA and replacement rhodopsin in a single virus, using the opsin promoter to restrict *RHO301* expression to rod photoreceptors. Since this gene maintained rhodopsin levels and prevented retinal degeneration in the presence of siRNA301, we conclude that off-target effects of this siRNA, if they occur, do not jeopardize the health of the retina. Nevertheless, it might be safer to embed the siRNA in a microRNA and express it in the same transcript as *RHO301*, thus restricting expression to photoreceptors. Georgiadis and coworkers have used an AAV-delivered microRNA to knock down *Prph2* mRNA in the mouse retina (Georgiadis *et al.*, 2011). In our current construct, expression of the siRNA is driven by the H1 RNA polymerase III promoter. To achieve more balanced expression of the two components, it might be better to express the siRNA as a microRNA encoded in the 3′ UTR of the *RHO* cDNA. This approach has led to long-term protection in a mouse model of autosomal dominant liver disease caused by the *PiZ* allele of α_1-antitrypsin (Mueller *et al.*, 2012).

Although this two-in-one gene therapy approach should work for other class 2 *RHO* mutations, efficacy must be documented in other animal models of ADRP. Preservation of central vision in the human eye will almost certainly require rescue of perimacular rod photoreceptors, and this would require testing in larger animals with cone-rich central retinas. We are taking steps in these directions.

Acknowledgments

The authors acknowledge support by the Foundation Fighting Blindness and the Shaler-Richardson endowment; by NIH grants EY13729, EY11123, EY08571, and EY020905 (to M.S.G.); and by grants from the Macular Vision Research Foundation, Eldon Family Foundation, and Vision for Children and Research to Prevent Blindness, Inc. for partial support of this work.

Author Disclosure Statement

W.W.H. and the University of Florida have a financial interest in the use of AAV therapies, and own equity in a company (AGTC Inc.) that might, in the future, commercialize some aspects of this work.

References

Cao, W., Wen, R., Li, F., *et al.* (1997). Mechanical injury increases bFGF and CNTF mRNA expression in the mouse retina. Exp. Eye Res. 65, 241–248.

Cashman, S.M., Binkley, E.A., and Kumar-Singh, R. (2005). Towards mutation-independent silencing of genes involved in retinal degeneration by RNA interference. Gene Ther. 12, 1223–1228.

Chadderton, N., Millington-Ward, S., Palfi, A., *et al.* (2009). Improved retinal function in a mouse model of dominant retinitis pigmentosa following AAV-delivered gene therapy. Mol. Ther. 17, 593–599.

Daiger, S.P., Bowne, S.J., and Sullivan, L.S. (2007). Perspective on genes and mutations causing retinitis pigmentosa. Arch. Ophthalmol. 125, 151–158.

Dryja, T.P., McGee, T.L., Reichel, E., *et al.* (1990). A point mutation of the rhodopsin gene in one form of retinitis pigmentosa. Nature 343, 364–366.

Flannery, J.G., Zolotukhin, S., Vaquero, M.I., *et al.* (1997). Efficient photoreceptor-targeted gene expression *in vivo* by recombinant adeno-associated virus. Proc. Natl. Acad. Sci. U.S.A. 94, 6916–6921.

Frederick, J.M., Krasnoperova, N.V., Hoffmann, K., *et al.* (2001). Mutant rhodopsin transgene expression on a null background. Invest. Ophthalmol. Vis. Sci. 42, 826–833.

Georgiadis, A., Tschernutter, M., Bainbridge, J.W., *et al.* (2011). AAV-mediated knockdown of peripherin-2 *in vivo* using miRNA-based hairpins. Gene Ther. 17, 486–493.

Gorbatyuk, M.S., Pang, J.J., Thomas, J., *et al.* (2005). Knockdown of wild-type mouse rhodopsin using an AAV vectored ribozyme as part of an RNA replacement approach. Mol. Vis. 11, 648–656.

Gorbatyuk, M., Justilien, V., Liu, J., *et al.* (2007a). Preservation of photoreceptor morphology P23H rats using an allele independent and function in ribozyme. Exp. Eye Res. 84, 44–52.

Gorbatyuk, M., Justilien, V., Liu, J., *et al.* (2007b). Suppression of mouse rhodopsin expression *in vivo* by AAV mediated siRNA delivery. Vis. Res. 47, 1202–1208.

Gorbatyuk, M.S., Hauswirth, W.W., and Lewin, A.S. (2008). Gene therapy for mouse models of ADRP. Adv. Exp. Med. Biol. 613, 107–112.

Gorbatyuk, M.S., Knox, T., Lavail, M.M., *et al.* (2010). Restoration of visual function in P23H rhodopsin transgenic rats by gene delivery of BiP/Grp78. Proc. Natl. Acad. Sci. U.S.A. 107, 5961–5966.

Hartong, D.T., Berson, E.L., and Dryja, T.P. (2006). Retinitis pigmentosa. Lancet 368, 1795–1809.

Huber, G., Beck, S. C., Grimm, C., *et al.* (2009). Spectral domain optical coherence tomography in mouse models of retinal degeneration. Invest. Ophthalmol. Vis. Sci. 50, 5888–5895.

Kaushal, S., and Khorana, H.G. (1994). Structure and function in rhodopsin. 7. Point mutations associated with autosomal dominant retinitis pigmentosa. Biochemistry 33, 6121–6128.

Kiang, A.S., Palfi, A., Ader, M., *et al.* (2005). Toward a gene therapy for dominant disease: Validation of an RNA interference-based mutation-independent approach. Mol. Ther. 12, 555–561.

Laemmli, U.K. (1970). Cleavage of structural proteins during the assembly of the head of bacteriophage T4. Nature 227, 680–685.

Lem, J., Krasnoperova, N.V., Calvert, P.D., *et al.* (1999). Morphological, physiological, and biochemical changes in rhodopsin knockout mice. Proc. Natl. Acad. Sci. U.S.A. 96, 736–741.

Lewin, A.S., Drenser, K.A., Hauswirth, W.W., *et al.* (1998). Ribozyme rescue of photoreceptor cells in a transgenic rat model of autosomal dominant retinitis pigmentosa. Nat. Med. 4, 967–971.

Li, C., Xiao, P., Gray, S.J., *et al.* (2011). Combination therapy utilizing shRNA knockdown and an optimized resistant transgene for rescue of diseases caused by misfolded proteins. Proc. Natl. Acad. Sci. U.S.A. 108, 14258–14263.

Lin, J.H., Li, H., Yasumura, D., *et al.* (2007). IRE1 signaling affects cell fate during the unfolded protein response. Science 318, 944–949.

Mao, H., James, T., Jr., Schwein, A., *et al.* (2011). AAV delivery of wild-type rhodopsin preserves retinal function in a mouse model of autosomal dominant retinitis pigmentosa. Hum. Gene Ther. 22, 567–575.

Mendes, H.F., van der Spuy, J., Chapple, J.P., and Cheetham, M.E. (2005). Mechanisms of cell death in rhodopsin retinitis pigmentosa: Implications for therapy. Trends Mol. Med. 11, 177–185.

Millington-Ward, S., Chadderton, N., O'Reilly, M., *et al.* (2011). Suppression and replacement gene therapy for autosomal dominant disease in a murine model of dominant retinitis pigmentosa. Mol. Ther. 19, 642–649.

Morris, M.B., Dastmalchi, S., and Church, W.B. (2009). Rhodopsin: Structure, signal transduction and oligomerisation. Int. J. Biochem. Cell Biol. 41, 721–724.

Mueller, C., Tang, Q., Gruntman, A., *et al.* (2012). Sustained miRNA-mediated knockdown of mutant AAT with simultaneous augmentation of wild-type AAT has minimal effect on global liver miRNA profiles. Mol. Ther. 20, 590–600.

Mussolino, C., Sanges, D., Marrocco, E., *et al.* (2011). Zinc-finger-based transcriptional repression of rhodopsin in a model of dominant retinitis pigmentosa. EMBO Mol. Med. 3, 118–128.

Noorwez, S.M., Kuksa, V., Imanishi, Y., *et al.* (2003). Pharmacological chaperone-mediated *in vivo* folding and stabilization of the P23H-opsin mutant associated with autosomal dominant retinitis pigmentosa. J. Biol. Chem. 278, 14442–14450.

Noorwez, S.M., Malhotra, R., McDowell, J.H., *et al.* (2004). Retinoids assist the cellular folding of the autosomal dominant retinitis pigmentosa opsin mutant P23H. J. Biol. Chem. 279, 16278–16284.

Olsson, J.E., Gordon, J.W., Pawlyk, B.S., *et al.* (1992). Transgenic mice with a rhodopsin mutation (Pro23His): A mouse model of autosomal dominant retinitis pigmentosa. Neuron 9, 815–830.

O'Reilly, M., Palfi, A., Chadderton, N., *et al.* (2007). RNA interference-mediated suppression and replacement of human rhodopsin *in vivo*. Am. J. Hum. Genet. 81, 127–135.

Phelan, J.K., and Bok, D. (2000). A brief review of retinitis pigmentosa and the identified retinitis pigmentosa genes. Mol. Vis. 6, 116–124.

Sakami, S., Maeda, T., Bereta, G., *et al.* (2011). Probing mechanisms of photoreceptor degeneration in a new mouse model of the common form of autosomal dominant retinitis pigmentosa due to P23H opsin mutations. J. Biol. Chem. 286, 10551–10567.

Saliba, R.S., Munro, P.M., Luthert, P.J., and Cheetham, M.E. (2002). The cellular fate of mutant rhodopsin: Quality control, degradation and aggresome formation. J. Cell Sci. 115, 2907–2918.

Smith, A.J., Bainbridge, J.W., and Ali, R.R. (2009). Prospects for retinal gene replacement therapy. Trends Genet. 25, 156–165.

Sullivan, J.M., Pietras, K.M., Shin, B.J., and Misasi, J.N. (2002). Hammerhead ribozymes designed to cleave all human rod opsin mRNAs which cause autosomal dominant retinitis pigmentosa. Mol. Vis. 8, 102–113.

Sung, C.H., Makino, C., Baylor, D., and Nathans, J. (1994). A rhodopsin gene mutation responsible for autosomal dominant retinitis pigmentosa results in a protein that is defective in localization to the photoreceptor outer segment. J. Neurosci. 14, 5818–5833.

Tam, B.M., and Moritz, O.L. (2006). Characterization of rhodopsin P23H-induced retinal degeneration in a *Xenopus laevis* model of retinitis pigmentosa. Invest. Ophthalmol. Vis. Sci. 47, 3234–3241.

Tan, E., Wang, Q., Quiambao, A.B., *et al.* (2001). The relationship between opsin overexpression and photoreceptor degeneration. Invest. Ophthalmol. Vis. Sci. 42, 589–600.

Timmers, A.M., Zhang, H., Squitieri, A., and Gonzalez-Pola, C. (2001). Subretinal injections in rodent eyes: Effects on electrophysiology and histology of rat retina. Mol. Vis. 7, 131–137.

Wilson, J.H., and Wensel, T.G. (2003). The nature of dominant mutations of rhodopsin and implications for gene therapy. Mol. Neurobiol. 28, 149–158.

Wu, T.H., Ting, T.D., Okajima, T.I., *et al.* (1998). Opsin localization and rhodopsin photochemistry in a transgenic mouse model of retinitis pigmentosa. Neuroscience 87, 709–717.

Zolotukhin, S., Potter, M., Zolotukhin, I., *et al.* (2002). Production and purification of serotype 1, 2, and 5 recombinant adeno-associated viral vectors. Methods 28, 158–167.

Address correspondence to:
Dr. Alfred S. Lewin
P.O. Box 100266
University of Florida
Gainesville, FL 32610-0266

E-mail: Lewin@ufl.edu

Received for publication November 23, 2011;
accepted after revision January 29, 2012.
Published online: January 30, 2012.